Comparison between the Q criterion and Rortex in the application of an in-stream structure

Cite as: Phys. Fluids **31**, 121701 (2019); https://doi.org/10.1063/1.5124245
Submitted: 16 August 2019 • Accepted: 12 November 2019 • Published Online: 05 December 2019

Jie-min Zhan (詹杰民), **Yu-tian Li** (李雨田), **Wing-hong Onyx Wai** (韋永康), **et al.**

Physics of Fluids LETTER scitation.org/journal/phf

Comparison between the Q criterion and Rortex in the application of an in-stream structure

Cite as: Phys. Fluids 31, 121701 (2019); doi: 10.1063/1.5124245
Submitted: 16 August 2019 • Accepted: 12 November 2019 •
Published Online: 5 December 2019

Jie-min Zhan (詹杰民),[1] Yu-tian Li (李雨田),[1] Wing-hong Onyx Wai (韋永康),[2] and Wen-qing Hu (胡文清)[1,a)]

AFFILIATIONS

[1]Department of Applied Mechanics and Engineering, Sun Yat-sen University, Guangzhou, China
[2]Department of Civil and Environmental Engineering, The Hong Kong Polytechnic University, Hong Kong, China

[a)]**Electronic mail:** huwq6@mail.sysu.edu.cn

ABSTRACT

A newly proposed vortex identification method, namely, Rortex, is used to visualize the vortex structures around an in-stream deflector with a large eddy simulation. A comparison with the well-known vortex identification method, the Q criterion, indicates that the Q criterion and Rortex can both capture the main vortex structures in the flow field. However, both the modified Q criterion and the wavelet analysis reveal that Rortex excludes the shear information on the deposited sand surface, while the Q criterion cannot. As a result, Rortex is more suitable for vortex identification.

Recently, a new vortex definition, namely, Rortex,[1–3] was proposed by Liu and his collaborators. Unlike previous methods proposed by many researchers,[4–6] which are based on velocity gradient tensor, Rortex has a definite physical meaning due to different decomposition of the velocity gradient tensor.[7,8] The objective of this study is to investigate the validity and advancement of Rortex in a complex practical problem, other than in DNS cases, in an intuitive way. Three methods, Rortex, the Q criterion,[4] and the modified Q criterion proposed in this paper, are chosen to visualize the vortex structures around the deflector (commonly used as an in-stream structure in open channels) in an equilibrium deformed bed condition obtained from experiments. The open channel scouring experiment was selected as the research object because of the complex flow structure and the existence of a great amount of vortex generation and transportation. Due to the presence of in-stream structures, the flow pattern becomes complicated and unsteady, and the flow structure is completely three-dimensional.[9] Unlike predictions via the traditional sediment transport equation,[10–12] this type of flow structure induces additional and different bed scouring characteristics. The generation and transportation of vortices affect sediment transport. Hence, it is essential to perform vortex visualization in the postprocessing part of design and analysis.

λ, the eigenvalues of the velocity gradient tensor, are computed by solving the cubic characteristic polynomial $\det(\nabla\vec{\mathbf{v}} - \lambda\mathbf{I}) = 0$, which can be written as

$$\lambda^3 + P\lambda^2 + Q\lambda + R = 0, \tag{1}$$

where P, Q, and R are three invariants of the velocity gradient tensor and $\mathbf{I}$ is the identity matrix. The vortex identification method based on invariants of the characteristic equation [Eq. (1)] has Galilean invariance. Furthermore, the velocity gradient ($\nabla\vec{\mathbf{v}}$) can be decomposed into two parts as follows:

$$\nabla\vec{\mathbf{v}} = \frac{1}{2}\left(\nabla\vec{\mathbf{v}} + \nabla\vec{\mathbf{v}}^{\mathrm{T}}\right) + \frac{1}{2}\left(\nabla\vec{\mathbf{v}} - \nabla\vec{\mathbf{v}}^{\mathrm{T}}\right) = \mathbf{S} + \mathbf{\Omega}, \tag{2}$$

where $\mathbf{S}$ is the symmetric part known as the rate of strain and $\mathbf{\Omega}$ is the antisymmetric part known as the vorticity tensor.

The Q criterion is directly derived based on the second invariant Q of the velocity gradient tensor given in Eq. (1) with the following expression:

$$Q = \frac{1}{2}\left(\|\mathbf{\Omega}\|^2 - \|\mathbf{S}\|^2\right), \tag{3}$$

where $Q > 0$ represents the existence of a vortex. According to the definition, the Q criterion defines vortices as areas where the vorticity magnitude is greater than the magnitude of the rate of strain.

Rortex, which represents the local fluid rotation, was proposed by Ref. 1. First, the local rotation axis $\vec{\mathbf{r}}$ is determined by computing the eigenvector corresponding to the real eigenvalue,

$$\nabla\vec{\mathbf{v}}\cdot\vec{\mathbf{r}} = \lambda_r\vec{\mathbf{r}}. \tag{4}$$

Then, after a coordinate rotation $\mathbf{Q}$, the local coordinate system with the rotation axis $\vec{\mathbf{r}}$ as the Z axis is established, and the rotation intensity can be obtained in the local coordinate system,

$$\nabla\vec{\mathbf{V}} = \mathbf{Q}\nabla\vec{\mathbf{v}}\mathbf{Q}^{\mathrm{T}} = \begin{bmatrix} \frac{\partial U}{\partial X} & \frac{\partial U}{\partial Y} & 0 \\ \frac{\partial V}{\partial X} & \frac{\partial V}{\partial Y} & 0 \\ \frac{\partial W}{\partial X} & \frac{\partial W}{\partial Y} & \frac{\partial W}{\partial Z} \end{bmatrix}. \tag{5}$$

The axis of rotation $\vec{\mathbf{r}}$ is the direction of R. The expression is as follows:

$$\begin{aligned} R &= \begin{cases} 2(\beta-\alpha), & \alpha^2-\beta^2<0, \\ 0, & \alpha^2-\beta^2\geq 0, \end{cases} \\ \alpha &= \frac{1}{2}\sqrt{\left(\frac{\partial V}{\partial Y}-\frac{\partial U}{\partial X}\right)^2+\left(\frac{\partial V}{\partial X}+\frac{\partial U}{\partial Y}\right)^2}, \\ \beta &= \frac{1}{2}\left(\frac{\partial V}{\partial X}-\frac{\partial U}{\partial Y}\right), \\ \vec{\mathbf{R}} &= R\vec{\mathbf{r}}. \end{aligned} \tag{6}$$

Unlike the previous decomposition of the velocity gradient, $\nabla\vec{\mathbf{V}}$ can be decomposed into the pure rotation part and the rest as follows:

$$\nabla\vec{\mathbf{V}} = \vec{\mathbf{R}} + \overrightarrow{\mathbf{NR}}, \tag{7}$$

where $\vec{\mathbf{R}}$ stands for the local rigid rotation and $\overrightarrow{\mathbf{NR}}$ represents the nonrotational part. Apart from the fact that $\vec{\mathbf{R}}$ can better represent the fluid rotation effect, $\overrightarrow{\mathbf{NR}}$ has a chance of expressing the effect of shear and convected velocity.

The open channel scouring experiment was conducted in a recirculating flume located in the Hydraulics Laboratory at the Hong Kong Polytechnic University. The width of the flume was 0.2 m, and the length was 9 m. The flume slope was 0.007. For this case, the flow depth D = 0.055 m, the average inlet velocity was 0.1 m/s, and the sediment layer was 0.03 m thick. Uniform-sized sand (d_{50} = 0.5 mm) was used in this experiment.

The bed topography was measured through an automatic measure system (Fig. 1). The accuracy of the system was ±0.1 mm for horizontal displacements and ±2 mm for vertical measurements. All the sample points for topography were 5 mm apart in the streamwise and transverse directions. The rectangular deflector with a thickness of 0.06 m and a width of 0.08 was 5 m away from the inlet.

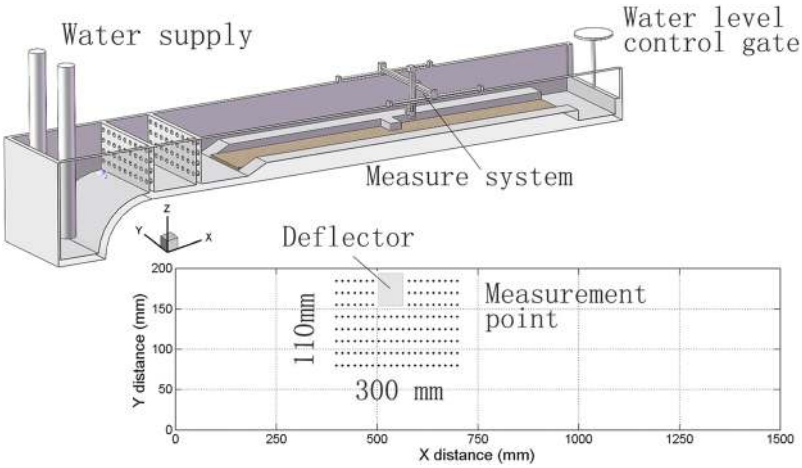

FIG. 1. Recirculating flume and automatic measure system.

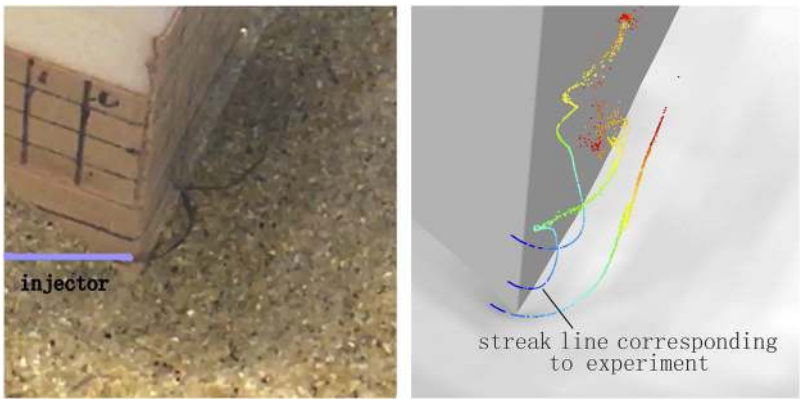

FIG. 2. Streak line comparison between experimental (left) and numerical (right) results.

The commercial software ANSYS Fluent is used for the numerical simulation. The volume of fluid (VOF) model with the geo-reconstruct method is used for capturing the free surface. The large eddy simulation (LES) turbulence model with the dynamic Smagorinsky-Lilly subgrid-scale model is used, and the Werner-Wengle wall functions are adopted for the near-wall treatment. The SIMPLE method is used to couple the pressure and velocity. The spatial discretization method is bounded central differencing, and the time discretization method is first order implicit. The computational domain is meshed using about 3.9×10^6 cells. The average Y^+ is about 8, while the other two directions are about 2 times larger. The velocity profile at the inlet boundary is obtained from a straight channel numerical simulation.

An eigenvalue-based method is used to calculate the Rortex value in a relatively efficient way. The Intel math kernel library (MKL) is used for matrix-related calculations. To implement the above two points in ANSYS Fluent, a method of calling a dynamic link library (DLL) with user defined functions (UDF) is adopted. With this method, the value of Rortex and its three xyz components at each grid point can be obtained.

The reliability of the numerical simulation is verified by comparing with the streak lines observed in our open channel scouring experiment (Fig. 2). The particle track method is adopted in the numerical simulation to get the streak lines at the points near the bottom around the corner. Compared with the streak line observed from the experiment using a dye tracer, the

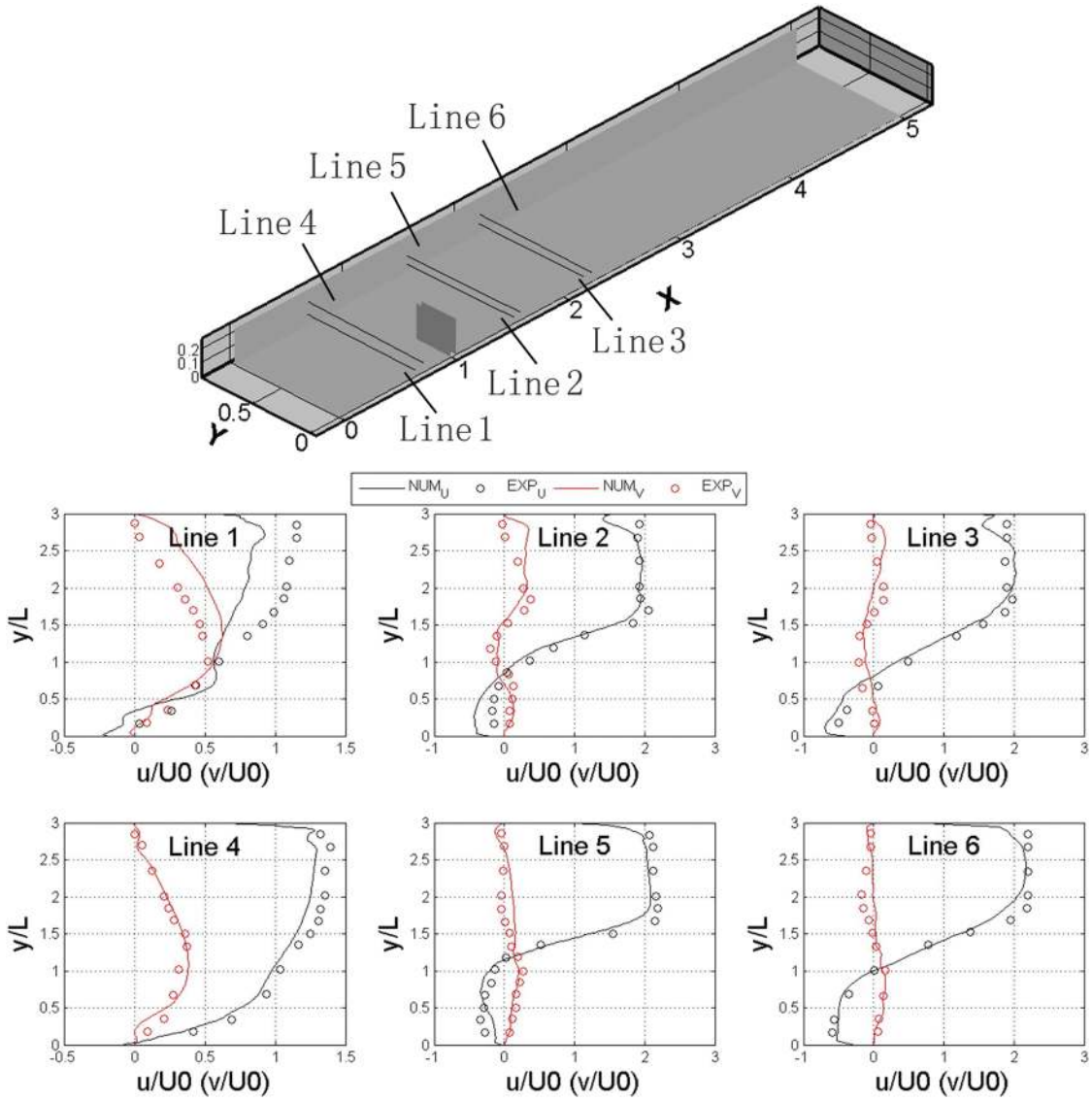

FIG. 3. Streamwise and spanwise velocity comparison.

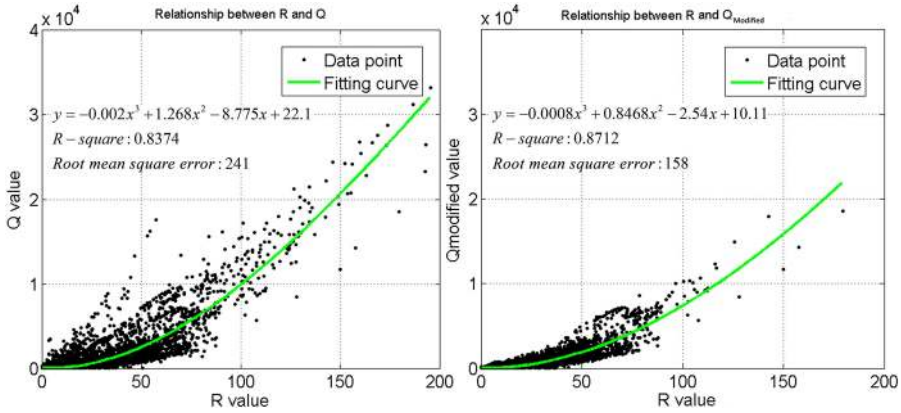

FIG. 4. Relationship between Rortex and Q.

corresponding numerical streak lines were similar and both have a three-dimensional spiral shape. The differences may be due to the slight errors in the coordinates of the measuring point.

For a further model-validity verification purpose, the spur dike flow experiment conducted in Ref. 13 is studied. The whole length of the flume was 18 m, and it was 0.9 m wide and 0.4 m deep. The computation setting is the same as described above; it has the same Y^+ except the computational domain is meshed using about 4.9×10^6 cells. Figure 3 presents the comparisons of streamwise velocity and spanwise velocity intensities between the experimental and numerical results along lines 1 to 6. As shown in Fig. 3, the simulation was generally consistent with the measurement, except at line 1, which may be due to the deviation of the velocity profile at the inlet boundary between the computational model and the experiment condition. This proves the numerical model is reliable.

Extracting the Rortex and Q values of each cell in the open channel scouring case, plotting these two types of values in the X-Y frame, we find that there is a correlation between them in the left picture of Fig. 4.

Part of the data points deviate from the fitting curve in the left picture of Fig. 4 possibly because the value of Q is based on the difference between vorticity and rate of strain, which cannot represent the pure rotation. To test this hypothesis, we choose to screen the Q criterion. The above refers to the symmetric tensor **S** with nine components, which can be divided into two classes: the relative extension and angle strain. We prefer to choose an angle strain that represents the cell deformation as the standard to screen the Q value; the screening equation is

$$Q_{Modified} = \begin{cases} Q & (angle\ strain < \alpha * \max(angle\ strain)) \\ 0 & (else) \end{cases}, \quad (8)$$

where the angle strain is $\frac{1}{2}\left(\frac{\partial u_i}{\partial x_j} + \frac{\partial u_j}{\partial x_i}\right)$. The parameter α of $Q_{Modified}$ affects the screening effect. As shown in Fig. 5, we find that 0.6 is the optimal value. The parameter α is set to 0.6 to exclude the major deformation part. After the screening, it is obvious in the right picture of Fig. 4 that the point of greatest deviation is suppressed, and the degree of correlation between Q and Rortex is enhanced. The deformation could cause the Q value to be misevaluated at some point. However, the Rortex value excludes deformation and is unaffected.

After different Rortex values are tested to display the vortex structures, the Rortex value is determined to be 25, and the corresponding Q value is 400 according to the above correlation equation between Rortex and Q. In general, except for the shear stress layer area and deposited sand surface (area 1 and area 2 in Fig. 6, respectively), the vortical structures shown by the two methods are similar. In the experiment, the dye tracer indicates that there is no vortex structure near the surface of the sand deposition; hence, the vortical structures shown by the Q value are not correct in this area. Figure 6 shows the detailed vortex structures near the deflector by Q, Rortex, and $Q_{Modified}$. After screening the Q value, the $Q_{Modified}$ result obviously improved near the deposited sand surface. There are almost no vortices existing on the scouring slope, which is the same as the Rortex results. It is also consistent with the phenomena observed in the open channel scouring experiment.

As shown in Fig. 7, the horseshoe vortex system (HV system) can be observed above the bed along the outer edge of the scouring slope. Experiments[14,15] and numerical simulations[16] have shown that the HV system plays an important role in the development of the scouring slope. The vector property of Rortex provides a new

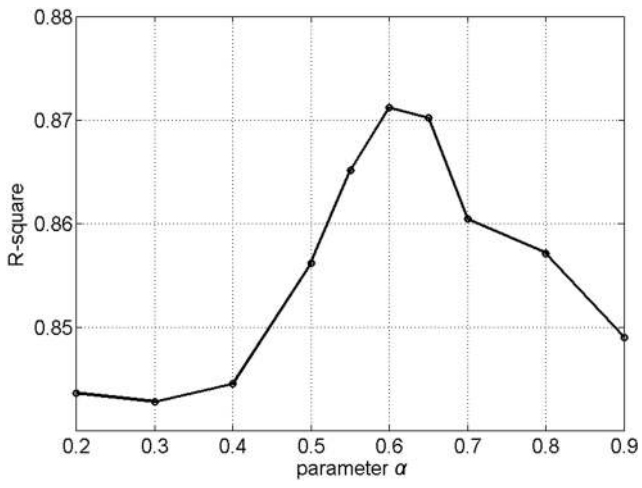

FIG. 5. Influence of the parameter α on the fitting effect.

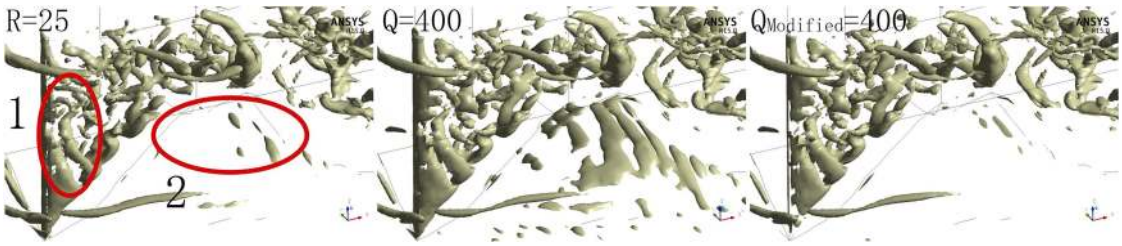

FIG. 6. Differences among the Rortex, Q criterion, and modified Q criterion results.

insight into the HV system. The scatter diagram of Rortex on a deformed surface 0.05D above the bed is shown in Fig. 8. The size of each point is determined by the magnitude of Rortex, and the color is determined by r_θ, which represents the angle between Rortex and the bed,

$$r_\theta = \left|90^\circ - \left\langle \vec{\mathbf{R}}, \vec{n_b} \right\rangle\right|, \tag{9}$$

where $\vec{n_b}$ is the normal vector of the local bed surface. As shown in Fig. 8, large wall shear stress occurs near the edge of the scouring slope; meanwhile, the HV system (the dotted area) is observed along the outer edge of the scouring slope. Furthermore, the color of the HV system shows that the rotation axes of the vortices in the system are mainly parallel to the sand bed surface. This series of tangential vortices drives the water above the sand bed surface to rotate on the normal plane, thus affecting the wall shear stress of the bed. This may explain the influence mechanism of the HV system on the development of the scouring slope.

According to the vortex visualization based on the Rortex value, there are two main paths of vortex shedding near the deflector. One originates from the shear stress layer near the edge of the deflector,

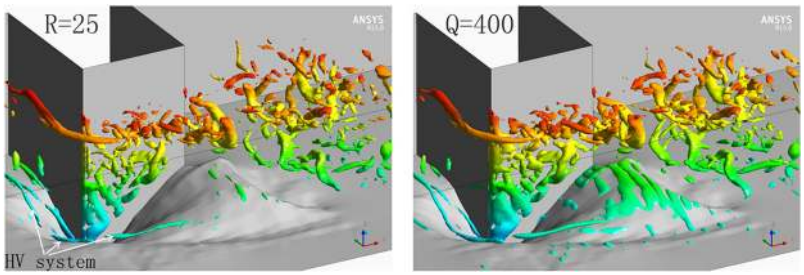

FIG. 7. Comparisons of the vortex structures induced by the in-stream structures.

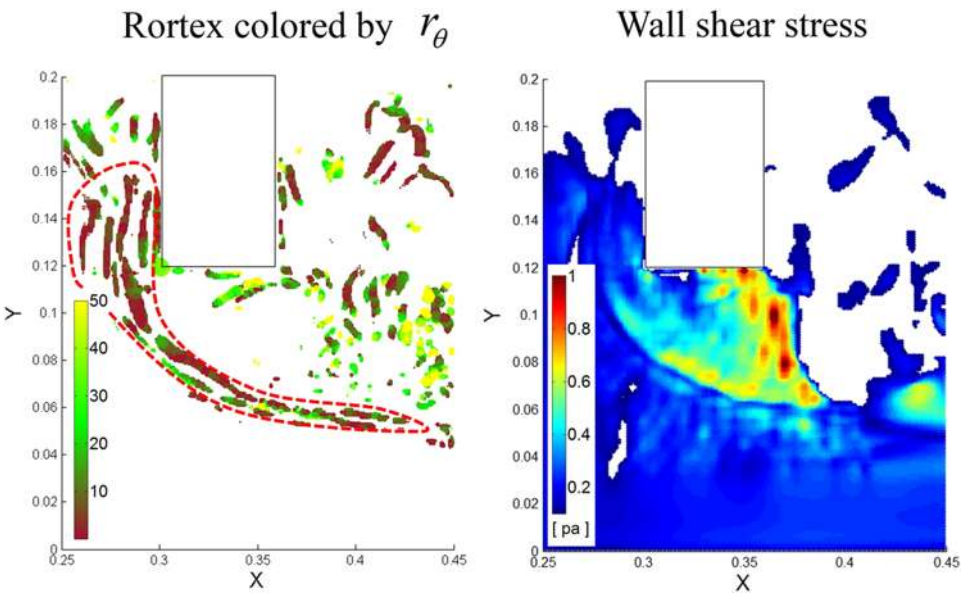

FIG. 8. Left: Rortex on a deformed surface 0.05D above the bed; right: wall shear stress of the bed.

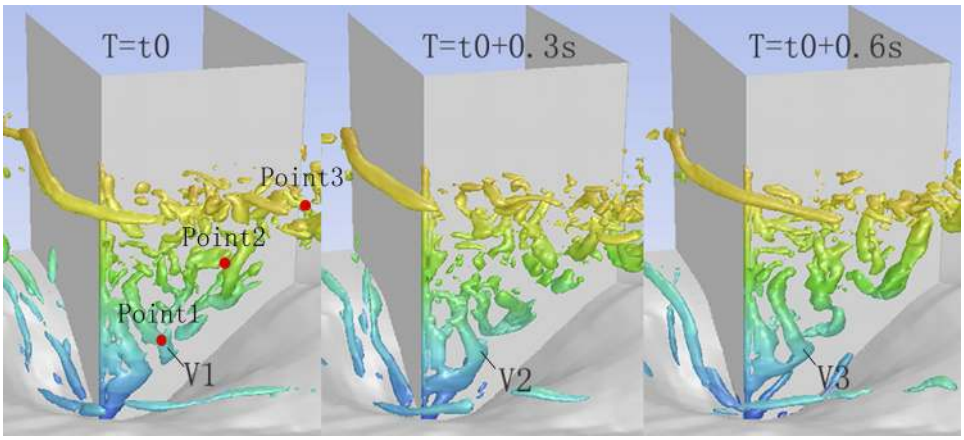

FIG. 9. Vortex visualization by Rortex near the deflector.

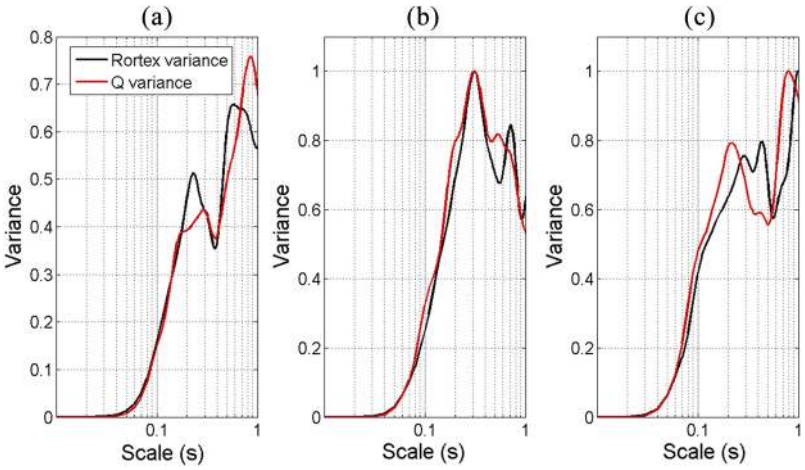

FIG. 10. Wavelet variance of Rortex and Q criterion. (a) Point 1; (b) Point 2; (c) Point 3.

and the other originates from the spiral flow at the bottom of the scour hole. In the downstream area, the two groups of vortices blend together and generate a new vortex group. Here, three points (red points in Fig. 9) inside the vortex generation, transportation, and interaction regions were monitored for the characteristics of spiral flow.

Most phenomena in turbulence problems can be represented as nonstationary series, which exhibit not only trends but also periodic randomness and abruptness. For the study of this kind of nonstationary time series, wavelet analysis can clearly reveal the various changing periods hidden in the time series and fully reflect the changing trend of the system in different time scales. The main period of the signal can be found by the wavelet variance, i.e., the wavelet energy graph. Therefore, the Q value and Rortex value at the three points are analyzed by a wavelet transform, and Morlet is used as the wavelet basis. In Fig. 10(a) (Point 1) and Fig. 10(b) (Point 2), the main periods of the minimum scale of Rortex are 0.23 s and 0.3 s, respectively, which are consistent with the 0.3 s vortex generation period directly observed in Fig. 9. The minimum main period of Q criterion in Fig. 10(a) is not clear, ranging from 0.17 s to 0.3 s. The first peak of Q criterion in Fig. 10(b) is consistent with that of Rortex. In Fig. 10(c) (Point 3), both Rortex and Q criterion deviate from 0.3 s due to the interaction of vortices. Comparing the local average angle strain rates at the three points in Table I, the Q criterion and Rortex capture the same main period at Point 2, which has the smallest average angle strain rate. This further confirms that the Q criterion is affected by shear deformation, as discussed previously.

In general, the wavelet analysis of Q criterion and Rortex can capture periodic phenomena with a period around 0.3 s. Furthermore, Rortex can give a clearer main period value than Q criterion inside the high deformation region, which confirms the accuracy of Rortex in capturing physical phenomena.

In conclusion, the comparison between Rortex and Q criterion reveals that Rortex eliminates the shear deformation and can

TABLE I. Local average angle strain rate.

	Point 1	Point 2	Point 3
Average angle strain (1/s)	56	25	38

represent pure local rotation. The screened Q, i.e., $Q_{Modified}$, gives a similar result as Rortex, which confirms the above view. The vector property of Rortex improves the understanding of the development of the scouring slope. Through wavelet analysis, both Rortex and Q criterion give the same main period in the low deformation region, but Rortex could give a clear main period in the high deformation region, while Q criterion cannot. Benefiting from the clear physical meaning of Rortex, the accurate flow data from the LES can be processed to obtain an accurate vortex structure diagram that can facilitate the analysis of the generation and transport of vortices and their impact on the flow field.

This work is supported by the National Project of China (Grant No. 6140206040301), the Fundamental Research Funds for the Central Universities of China (Grant No. 17LGJC41) and the Hong Kong Research Grants Council (Grant No. 15274316).

REFERENCES

[1]C. Liu *et al.*, "Rortex—A new vortex vector definition and vorticity tensor and vector decompositions," Phys. Fluids **30**(3), 035103 (2018).
[2]Y. Gao and C. Liu, "Rortex based velocity gradient tensor decomposition," Phys. Fluids **31**(1), 011704 (2019).
[3]X. Dong, Y. Gao, and C. Liu, "New normalized Rortex/vortex identification method," Phys. Fluids **31**(1), 011701 (2019).
[4]J. C. R. Hunt, A. A. Wray, and P. Moin, "Eddies, streams, and convergence zones in turbulent flows," in *Proceedings of the Summer Program* (Center for Turbulence Research, 1988), pp. 193–208.
[5]M. S. Chong, A. E. Perry, and B. J. Cantwell, "A general classification of three-dimensional flow field," Phys. Fluids A **2**, 765–777 (1990).
[6]J. Jeong and F. Hussain, "On the identification of a vortex," Phys. Fluids **285**, 69–94 (1995).
[7]V. Kolář, "Vortex identification: New requirements and limitations," Int. J. Heat Fluid Flow **28**(4), 638–652 (2007).
[8]B. Sun, "A new additive decomposition of velocity gradient," Phys. Fluids **31**, 061702 (2019).
[9]M. Koken and G. Constantinescu, "An investigation of the dynamics of coherent structures in a turbulent channel flow with a vertical sidewall obstruction," Phys. Fluids **21**(8), 085104 (2009).
[10]F. Engelund and J. Fredsøe, "A sediment transport model for straight alluvial channels," Hydrol. Res. **7**(5), 293–306 (1976).
[11]J. D. Smith and S. R. McLean, "Spatially averaged flow over a wavy surface," J. Geophys. Res. **82**(12), 1735–1746, https://doi.org/10.1029/jc082i012p01735 (1977).
[12]L. C. van Rijn, "Sediment transport, Part II: Suspended load transport," J. Hydraul. Eng. **110**(11), 1613–1641 (1984).
[13]J. Jeon, J. Y. Lee, and S. Kang, "Experimental investigation of three-dimensional flow structure and turbulent flow mechanisms around a nonsubmerged spur dike with a low length-to-depth ratio," Water Resour. Res. **54**(5), 3530–3556, https://doi.org/10.1029/2017wr021582 (2018).
[14]B. W. Melville and A. J. Raudkivi, "Flow characteristics in local scour at bridge piers," J. Hydraul. Res. **15**(4), 373–380 (1977).
[15]J. Unger and W. H. Hager, "Down-flow and horseshoe vortex characteristics of sediment embedded bridge piers," Exp. Fluids **42**(1), 1–19 (2007).
[16]M. Koken and G. Constantinescu, "Flow and turbulence structure around a spur dike in a channel with a large scour hole," Water Resour. Res. **47**, 12, https://doi.org/10.1029/2011wr010710 (2011).